

Subthreshold Membrane Conductances Enhance Directional Selectivity in Vertebrate Sensory Neurons

Maurice J. Chacron^{1,2} and Eric S. Fortune^{3,4}

¹Department of Physiology, Center for Nonlinear Dynamics, and ²Department of Physics, McGill University, Montreal, Quebec, Canada; ³Departments of Psychological and Brain Sciences and ⁴Neuroscience, Johns Hopkins University, Baltimore, Maryland

Submitted 18 December 2009; accepted in final form 3 May 2010

Chacron MJ, Fortune ES. Subthreshold membrane conductances enhance directional selectivity in vertebrate sensory neurons. *J Neurophysiol* 104: 449–462, 2010. First published May 5, 2010; doi:10.1152/jn.01113.2009. Directional selectivity, in which neurons respond preferentially to one “preferred” direction of movement over the opposite “null” direction, is a critical computation that is found in the central nervous systems of many animals. Such responses are generated using two mechanisms: spatiotemporal convergence via pathways that differ in the timing of information from different locations on the receptor array and the nonlinear integration of this information. Previous studies have showed that various mechanisms may act as nonlinear integrators by suppressing the response in the null direction. Here we show, through a combination of mathematical modeling and *in vivo* intracellular recordings, that subthreshold membrane conductances can act as a nonlinear integrator by increasing the response in the preferred direction of motion only, thereby enhancing the directional bias. Such subthreshold conductances are ubiquitous in the CNS and therefore may be used in a wide array of computations that involve the enhancement of an existing bias arising from differential spatiotemporal filtering.

INTRODUCTION

A critical function of nervous systems is the extraction of behaviorally relevant features of sensory stimuli via computations in central brain circuits. Perhaps the most well known computation involves determining the direction of motion of a sensory stimulus. Neurons that respond selectively to a given direction of movement have been discovered in a variety of organisms ranging from insects to mammals (Borst and Egelhaaf 1989, 1990; Euler et al. 2002; Haag et al. 2004; Hubel and Wiesel 1962; Jagadeesh et al. 1997; Priebe and Ferster 2008; Srinivasan et al. 1999) and are thought to be a neural correlate of motion perception. Understanding the mechanisms by which neurons respond selectively to a given direction of motion has been the focus of intense investigation for the past 50 yr.

The mechanisms for direction selectivity rely on two fundamental operations (Reichardt and Wenking 1969). The first operation involves generating a directional bias by asymmetric filtering of information from at least two separate spatial locations within the receptive field. Many mechanisms can give rise to a directional bias, including dendritic integration (Euler et al. 2002), temporal delays (Haag et al. 2004; Jagadeesh et al. 1997), and synaptic depression (Carver et al. 2008; Chacron et al. 2009; Chance et al. 1998).

The second operation involves the nonlinear interaction of these inputs. Various types of nonlinearities have been proposed such as multiplication (Reichardt 1987), squaring (Adelson and Bergen 1985), shunting (Euler et al. 2002), and thresholding (Priebe and Ferster 2008; Priebe et al. 2004).

Perhaps the most widely known type of Reichardt detector is the one found in the visual system of insects (Borst and Egelhaaf 1989, 1990). In this detector, the directional bias is generated by delaying the output from one spatial position in the receptive field and the nonlinear integration is generated by a downstream multiplier. It is for this reason that the Reichardt detector found in the visual system of insects is sometimes referred to as a correlation-based detector in that it responds to inputs that are correlated. It is important to note that, as described in the preceding text, any asymmetric filtering followed by any nonlinear interaction of at least two spatially separate inputs will give rise to directional selectivity (Borst and Egelhaaf 1990; Reichardt 1987).

Weakly electric fish are particularly well-suited for the study of motion processing as these animals have been intensively studied for over 30 yr in relation to electrosensory processing and have unusually well characterized neural circuits (Fortune 2006; Maler et al. 1991). These animals produce electric fields using a specialized electric organ and can sense distortions of the self-generated electric field through an array of electroreceptors located in the skin (Fortune 2006). These electroreceptors project to pyramidal cells within the electrosensory lateral line lobe, which in turn project to the midbrain torus semicircularis (TS) (Maler et al. 1991), which is the equivalent of the mammalian inferior colliculus. Previous studies have shown that directional selectivity emerges at the level of the TS (Bastian 1981; Chacron et al. 2009; Ramcharitar et al. 2005, 2006) and that differences in the time constants of short-term depression most likely generated the necessary directional bias (Chacron et al. 2009).

Here we show that subthreshold membrane conductances can act as a nonlinear integrator in generating directionally biased responses in vertebrate sensory neurons. In contrast to previously proposed nonlinear integrators, these conductances act to enhance the response in the preferred direction only. Our study includes a generic mathematical model that we used to explore the ranges of parameters in which subthreshold conductances can enhance, attenuate, or have no effect a given directional bias. We then present experimental evidence that subthreshold conductances found in TS neurons of weakly electric fish can enhance directional biases by selective activation only when the object moves in the preferred direction. Finally, we use pharmacological techniques to better understand the nature of the ion channels that mediate the subthreshold conductance.

Address for reprint requests and other correspondence: E. S. Fortune, Dept. of Psychological and Brain Sciences, Johns Hopkins University, 3400 N. Charles St., Baltimore, MD, 21218. (E-mail: eric.fortune@jhu.edu).

METHODS

Animals

The weakly electric fish *Apteronotus leptorhynchus* was used in this study. Animals were obtained from tropical fish suppliers and acclimated in the laboratory setting for several days before being used for experiments according to published guidelines (Hitschfeld et al. 2009). The experimental procedures have been described in detail elsewhere (Bastian et al. 2002; Chacron 2006; Chacron and Bastian 2008; Chacron et al. 2009; Mehaffey et al. 2008; Toporikova and Chacron 2009). All procedures were approved by the institutional animal care and use committees of Marine Biological Laboratory, McGill University, and the Johns Hopkins University. Animal husbandry and all experimental procedures followed guidelines established by the Society for Neuroscience and the National Research Council.

Stimulation and recording

Intracellular recordings were made from torus semicircularis (TS) neurons within the most superficial five layers in intact, awake, behaving fish using patch pipettes, as has been described previously (Chacron et al. 2009; Rose and Fortune 1996). Data were acquired with a Cambridge Electronic Design Power1401 hardware and Spike2 software (Cambridge, UK). Neurons were held at various levels of polarization using DC current injected through the recording electrode; current injection ranged between -0.4 and $+0.2$ nA.

Stimuli included moving objects (Chacron et al. 2009; Ramcharitar et al. 2005, 2006) consisting of a 1.8 cm wide metal plate with a plastic coating on the side opposite to the animal. The object was actuated with a pen plotter (HP 7010B) and moved sinusoidally along the fish's rostrocaudal axis over a distance of 15 cm. The sinusoid was centered at the animal's midpoint and had a frequency of 0.25 Hz, corresponding to an average velocity of ~ 10 cm/s, which is the observed mean velocity of salient sensory images during prey capture behavior (Nelson and MacIver 1999) and within the velocities of error signals that the fish experience during refuge tracking behaviors (Cowan and Fortune 2007). These stimuli were repeated ≥ 20 times.

In other experiments, a small stationary dipole was positioned at different rostrocaudal positions to map a given neuron's receptive field. The dipole was used to deliver amplitude modulations of the animal's electric organ discharge (EOD) using previously established techniques (Bastian et al. 2002; Chacron 2006; Chacron et al. 2003, 2009). The stimuli consisted of 20 Hz sinusoidal amplitude modulations that lasted for 250 ms and were repeated every second ≥ 200 times (Chacron et al. 2009). Such stimuli have been previously shown to elicit reliable synaptic depression at electrosensory lateral line lobe to torus synapses (Fortune and Rose 2000). These studies have furthermore shown that the time constant of depression was independent of the frequency used. Responses to such stimuli were accumulated as peristimulus time histograms. The peak response at every stimulus cycle was fitted with a decaying exponential to obtain the depression time constant τ_i at a given position. The different time constants obtained at different positions were then used in a model (described in the following text) to predict the directional bias. We note that the same dipole was used as the moving object for the neurons for which we mapped the receptive field (Chacron et al. 2009).

Pharmacology

We blocked sodium channels by adding 2 mM QX-314 (Sigma-Aldrich, St. Louis, MO) to the internal pipette solution as was done previously (Fortune and Rose 2003). We blocked inhibition by adding 50 mM picrotoxin (PTX, Sigma-Aldrich) to the internal pipette solution. PTX has been previously shown to block chloride channels when applied intracellularly at these concentrations (Inomata et al.

1988). We used pressure to inject saline, mibefradil dihydrochloride (Mib; 1 mM, Sigma-Aldrich), NiCl_2 (1 mM, Sigma-Aldrich), and 2-amino-5-phosphonovaleric acid (APV; 1 mM, Sigma-Aldrich) into the brain. A patch pipette with a large tip diameter (~ 0.5 mM) was connected to a 50 ml syringe and advanced into the TS close to the recording pipette. Gentle pressure was then applied to the syringe to eject the drug without disrupting the intracellular recording.

Previous studies have shown that pressure injection leads to effective concentrations that are ≥ 10 times less at the recording site (Turner et al. 1994). Although NiCl_2 is a broad spectrum antagonist of calcium channels, Mib has been shown to be specific for T-type calcium channels at these concentrations (Bloodgood and Sabatini 2007; Mehrke et al. 1994). Intracellular recordings were successfully maintained during the injection of NiCl_2 and Mib in five neurons, thereby allowing a direct comparison of the postsynaptic potentials (PSPs) before and after injection. Directional selectivity was compared in neurons recorded extra- or intracellularly before and after the injection of saline, NiCl_2 , and Mib. These drugs were effective, as evidenced in the data, for ≥ 3 h after injection. For QX-314, we computed the directional selectivity index (DSI) from the membrane potential. We computed the DSI from the spike train for all other agents used.

Modeling

Our model is based on Hodgkin-Huxley formalism with the current balance equation

$$C \frac{dV}{dt} = -g_{\text{leak}}(V - E_{\text{leak}}) - g_{\text{T}} s_{\infty}^3(V) h(V)(V - E_{\text{Ca}}) + I(t)$$

$$\frac{dh}{dt} = \frac{h_{\infty}(V) - h}{\tau_h} \quad (1)$$

where C is the membrane capacitance, V is the transmembrane potential difference, g_{leak} and g_{T} are the leak and voltage-gated calcium channel conductances with reversal potentials E_{leak} and E_{Ca} , respectively. We chose to use model parameters for a calcium channel, but many other conductances, including subthreshold sodium conductances, would produce identical results. The calcium channel is assumed to activate in the subthreshold regime with negligible time constant, and the variable h is the inactivation variable. The activation and inactivation kinetics were fitted from previous experimental data on T-type calcium channels (Coulter et al. 1989; Rush and Rinzel 1994)

$$s_{\infty}(V) = \frac{1}{1 + \exp\left(-\frac{V + 63}{7.8}\right)} \quad (2)$$

$$h_{\infty}(V) = \frac{1}{0.5 + \sqrt{0.25 + \exp\left(-\frac{V + 82}{6.3}\right)}} \quad (3)$$

In our previous study (Chacron et al. 2009), we used a mathematical model that incorporated different time constants of synaptic depression from different spatial positions within the receptive field. We thus briefly describe this model here. The receptive field of the model neuron is one-dimensional and is composed of N "zones" of length 5 mm. The output of the i th zone is given by

$$O_i(t) = G_i \Theta(t - t_i) \exp\left(-\frac{t}{\tau_i}\right) \quad (4)$$

where t_i is the time at which the moving object first enters the i th zone, and $\Theta(t)$ is the Heaviside function [$\Theta(t) = 1$ if $t \geq 0$ and $\Theta(t) = 0$ otherwise]. Here G_i , τ_i are the gain and depression time constant associated with the i th zone, respectively. All simulations were done with a point moving object moving at a constant speed of 10 cm/s, which

corresponds to the velocity at which the animal moves during prey capture (Nelson and MacIver 1999). The input $I(t)$ was then taken as the sum of the inputs from all zones convolved with an alpha function (time constant, 20 ms). For all simulations, the gains G_i and depression time constants τ_i were obtained from experimental measurements as previously described (Chacron et al. 2009). We simulated this model using an Euler algorithm with integration time step $dt = 0.0025$ ms. Other parameter values used were $g_{\text{leak}} = 0.18 \mu\text{S}$, $E_{\text{leak}} = -70$ mV, $E_{\text{ca}} = 120$ mV, $C = 1 \mu\text{F}$, $\tau_h = 30$ ms. This model was used to generate the results described in Figs. 2, A–D, and 4.

In other simulations, the input $I(t)$ was taken to be composed of a bias term plus a time varying part the time course of which is an alpha function

$$I(t) = I_{\text{bias}} + A \frac{t}{\tau_\alpha} \exp\left(1 - \frac{t}{\tau_\alpha}\right) \quad (5)$$

where $\tau_\alpha = 6$ ms. We simulated the directional bias in the input by varying the parameter A . This parameter took the value A_p when the object moved in the preferred direction and took the value A_n when the object moved in the null direction. The input directional bias DI_{in} is then defined by

$$DI_{\text{in}} = \frac{A_p - A_n}{\max(A_p, A_n)} \quad (6)$$

The output directional bias was then defined as

$$DI_{\text{out}} = \frac{\Delta V_p - \Delta V_n}{\max(\Delta V_p, \Delta V_n)} \quad (7)$$

where ΔV_x is the maximum voltage depolarization caused by the input with amplitude A_x . We note that, to compute DI_{in} and DI_{out} , we had to perform a nonlinear operation in computing the maximum value. Comparing DI_{in} and DI_{out} allows us to gauge the effects of the nonlinear subthreshold conductance as $DI_{\text{in}} = DI_{\text{out}}$ for a linear system. We also simulated this model using an Euler algorithm with integration time step $dt = 0.0025$ ms. Other parameter values used were $g_{\text{leak}} = 0.18 \mu\text{S}$, $E_{\text{leak}} = -70$ mV, $E_{\text{ca}} = 120$ mV, $C = 1 \mu\text{F}$, $\tau_h = 30$ ms, and $I_{\text{bias}} = -1.1$ nA unless indicated otherwise. This model was used to generate the results described in Figs. 2, E–H, and 3.

Data analysis

Data from TS neurons and from the model with synaptic depression were analyzed similarly. The directional selectivity index (DSI) was computed as

$$DSI = \frac{R_{\text{HT}} - R_{\text{TH}}}{\max(R_{\text{HT}}, R_{\text{TH}})} \quad (8)$$

R_{HT} , R_{TH} are the maximum responses when the object moves from head to tail and from tail to head, respectively. We note that this definition differs slightly from that used by other authors (Jagadeesh et al. 1997; Priebe and Ferster 2008) and that this does not affect our results qualitatively. The DSI is thus 1 for a neuron that responds only when the object moves in one direction and 0 for a neuron that responds equally when the object moves in both the head-to-tail and tail-to-head directions. Spiking responses were accumulated as peristimulus time histograms and the maximum responses were taken to be the peak firing rates. We also computed DSI from the subthreshold membrane potential response with spikes removed: the maximum responses where then taken to be the maximum positive voltage deflections with respect to the resting membrane potential (i.e., the value when no stimulus is present) as before (Chacron et al. 2009). Spikes were removed by using a finite impulse response (FIR) filter with a 30 Hz cutoff frequency in Spike2. The mean square error $\langle \varepsilon^2 \rangle$ was defined as

$$\langle \varepsilon^2 \rangle = \sum_{i=1}^N (DSI_{i,\text{measured}} - DSI_{i,\text{predicted}})^2 \quad (9)$$

where $DSI_{i,\text{measured}}$ and $DSI_{i,\text{predicted}}$ are the values of DSI experimentally measured and predicted by the model, respectively. Here N is the data sample size ($n = 10$).

RESULTS

TS neurons display directional selectivity

We performed in vivo intracellular recordings from TS neurons ($n = 21$) while moving an object back and forth along the side of the animal (Fig. 1A). The majority of neurons,

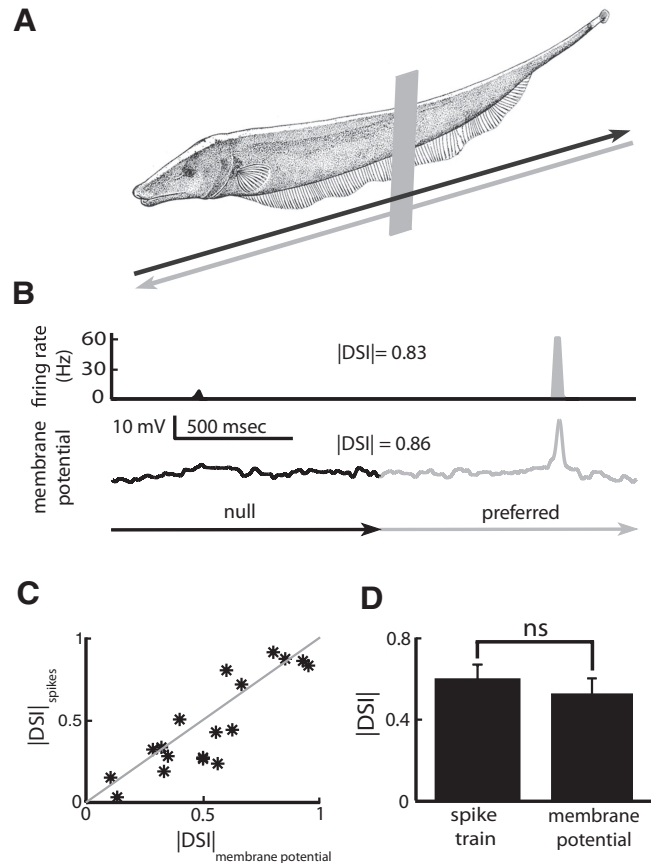


FIG. 1. The spiking and subthreshold membrane potential responses of TS neurons display identical directional biases. A: schematic of the experimental setup: a moving object (vertical gray bar) was moved sinusoidally back and forth lateral to the animal. Gray arrow, tail-to-head direction; black arrow, head-to-tail direction. B: example spiking (top) and membrane potential (bottom) of an example TS neuron averaged over stimulus trials. This neuron showed weak or no responses when the object moved from head to tail (black) and strong responses when the object moved from tail to head (gray). Directional selectivity was quantified by comparing the peak responses in both the spike train and membrane potential in both the preferred (i.e., the direction that gave rise to the greatest peak response) and null (i.e., the other direction) directions. The values of |directional selectivity index| (|DSI|) computed from the membrane potential and spike train were 0.86 and 0.83, respectively. C: |DSI| computed from the spike train plotted as a function of |DSI| computed from the membrane potential for our dataset. We observed a strong and significant correlation coefficient between both quantities ($R = 0.87$, $P \ll 10^{-3}$, $n = 18$) with most datapoints lying across the identity line (gray line). D: population-averaged |DSI| values obtained from the spike train (left) and subthreshold membrane potential (right) responses were not significantly different ($P = 0.4961$, sign-rank test, $n = 18$).

consistent with previous studies (Chacron et al. 2009; Ramcharitar et al. 2006), exhibited directional selectivity (Fig. 1*B*). An example neuron shown in Fig. 1*B* responded strongly when the object moved from tail to head (the preferred direction) and weakly when the object moved from head to tail (the null direction). The response in the preferred direction consisted of a large depolarization in the membrane potential response (Fig. 1*B*, bottom), which led to a large increase in firing rate (Fig. 1*B*, top). In contrast, the response in the null direction consisted of a small depolarization in the membrane potential response (Fig. 1*B*, bottom), which led to a small increase in firing rate (Fig. 1*B*, top).

We quantified the directional bias in both the intracellular and spiking responses of TS neurons using a previously established measure termed the DSI, which ranges between -1 (complete directional selectivity in the tail-to-head direction) to 1 (complete directional selectivity in the head-to-tail direction) with a value of 0 indicating no directional preference (Chacron et al. 2009). Because our concern here is understanding the mechanisms by which TS neurons display a directional bias rather than the particular direction to which they best respond to, we report values for the absolute directional selectivity index |DSII|, which ranges between 0 (no directional selectivity) and 1 (complete directional selectivity). We found a strong and significant correlation between |DSII| measured from the membrane potential and |DSII| measured from the spiking response (Fig. 1*C*; $R = 0.87$, $P \ll 10^{-3}$, $n = 18$). As a consequence, the population-averaged |DSII| values computed from the membrane potential and spike train were not significantly different from one another (Fig. 1*D*; $P = 0.4961$, sign-rank test, $n = 18$). This implies that the spiking threshold does not act as the nonlinear integrator here and therefore does not act to suppress the response in the null direction, which is contrary to what is seen in other systems (Priebe and Ferster 2008; Priebe et al. 2004). We conclude that nonlinear integration must instead occur in the subthreshold regime.

Subthreshold conductances can conserve, amplify, or attenuate underlying directional biases in a mathematical model

We have previously shown that differences in the time constant of depression from different spatial locations within a given neuron's receptive field generated the necessary directional bias in TS neurons (Chacron et al. 2009). The basic schematic for generating directional selectivity using two different time constants of depression is illustrated in Fig. 2*A*. When the object moves from the zone with the longest time constant to the zone with the shortest time constant, there is significant overlap between the two responses (Fig. 2*B*). In contrast, when the object moves from the zone with the shortest time constant to the zone with the longest time constants, the amount of overlap is significantly reduced (Fig. 2*C*). As a result, the sum of the two responses displays a greater maximum value in the former case and a lesser maximum value in the latter case (Fig. 2*D*).

This difference in the maximum value can be used to generate directionally biased responses through nonlinear mechanisms as previously described (Carver et al. 2008; Chance et al. 1998). It is important to note here that the maximum value of |DSII| that can be generated from this model is 0.5 . To see this, consider the case where the maximum value of the responses from each zone are both equal to $A > 0$.

Furthermore, let us assume there is total overlap between the two responses in the preferred direction and that there is no overlap in the null direction. As such, the maximum response amplitude of the summed input is then $A + A = 2A$ in the preferred direction and A in the null direction. It is then easy to show that $|DSII| = (2A - A)/(2A) = 0.5$. Furthermore, this is the maximum value that |DSII| can take as any less than total overlap between the responses will decrease the value of |DSII|. It is thus clear that this model alone cannot completely account for directional selectivity in TS neurons that display values of $|DSII| > 0.5$ such as the example neuron from Fig. 1 for which we obtained $|DSII| = 0.86$.

Here we are interested in understanding the nature of the nonlinear integrator in TS neurons that could potentially explain why we obtained values of |DSII| that were >0.5 . Because previous studies have shown that TS neurons can display large, all-or-none conductances that are active in the subthreshold regime (Fortune and Rose 1997, 2003), we therefore tested the hypothesis that such conductances act as the necessary nonlinear integrator responsible for the observed directional bias in the membrane potential of TS neurons. To test this idea, we started by building a model that consisted of a leak current and a voltage-gated calcium channel that activates in the subthreshold regime (Fig. 2*E*). Please note that our model did not contain any spiking currents because our data showed that the |DSII| computed from the spike train was on average equal to that computed from the membrane potential. For simplicity, we simulated the input directional bias by injecting alpha functions of different amplitudes A_p and A_n as an input rather than using the full model with synaptic depression (Fig. 2*E*) and computed the output directional bias DI_{out} from the model's membrane potential response.

We then tested the model's ability to act as a nonlinear integrator by comparing the output bias DI_{out} , which was computed from the voltage depolarizations ΔV_p and ΔV_n obtained in response to the inputs A_p and A_n , respectively (Fig. 2*E*). It is important to note that nonlinear operations must be used to compute both DI_{in} and DI_{out} . Comparing the values of DI_{in} and DI_{out} allows us to quantify the effects of the nonlinear subthreshold conductance as $DI_{in} = DI_{out}$ for any linear system. Figure 2*F* shows the output bias DI_{out} as a function of the input bias DI_{in} for different values of the active conductance. Without the active conductance, our model is a linear system and the output directional bias DI_{out} is thus always equal to the input directional bias DI_{in} . We found that increasing the active conductance initially increased the output directional bias DI_{out} for a given input directional bias DI_{in} , with increasing values of g_T being able to increase smaller and smaller input directional biases DI_{in} (Fig. 2*F*). However, further increasing the active conductance value caused the output directional bias to be actually less than the input directional bias (Fig. 2*F*). These results show that the output directional bias could reach values that were >0.5 .

To better understand these results, we specifically looked at three cases (Fig. 2*G*). In *case 1*, both the inputs cause voltage deflections that are below the activation threshold for the active conductance. In *case 2*, the larger input simulating movement in the preferred direction causes a voltage deflection that activates the conductance, whereas the smaller input simulating movement in the null direction does not. In *case 3*, both inputs cause voltage deflections that activate the conductance.

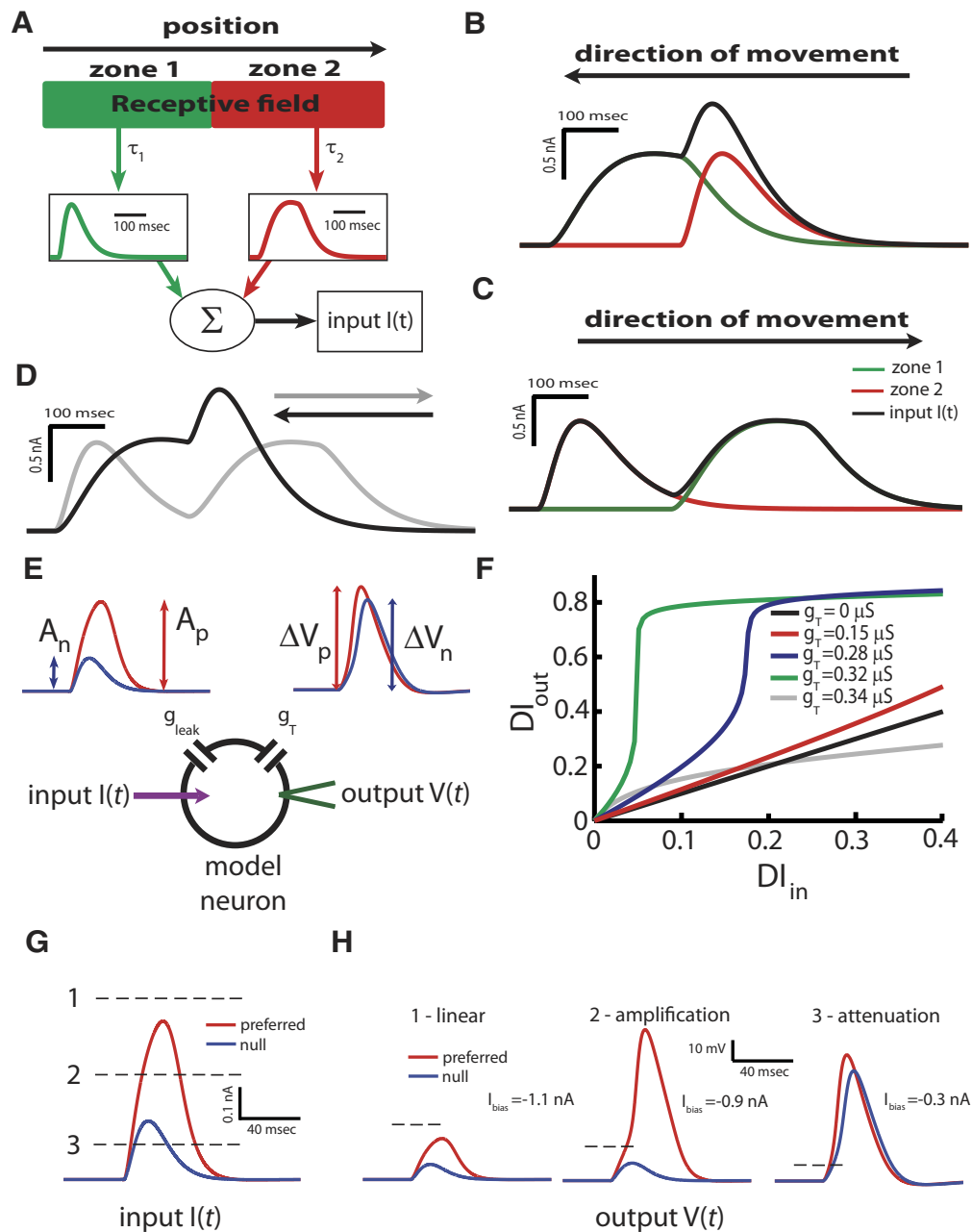


FIG. 2. Modeling the effects of a subthreshold T-type calcium channel on an existing directional bias. *A*: schematic of the receptive field of a hypothetical neuron that is composed of zones 1 and 2. Zones 1 and 2 differ in their responses to a moving object as they have different temporal profiles that are characterized by different time constants of decay τ_1 and τ_2 , respectively. These responses are summed to give rise to the input $I(t)$. The responses are illustrated for $\tau_1 = 10$ ms and $\tau_2 = 200$ ms. *B*: responses of zone 1 (green), zone 2 (red), and input $I(t)$ (black) when the object moves from right to left. *C*: responses of zone 1 (green), zone 2 (red), and input $I(t)$ (black) when the object moves from left to right. *D*: input $I(t)$ when the object moves from left to right (gray) and when the object moves from right to left (black). When the object moves from right to left, there is overlap between the responses from zones 1 and 2 because the object first moves through zone 2, which has the greatest time constant of decay, leading to a greater maximum value for the input $I(t)$. When the object moves from left to right, the amount of overlap between the responses of zones 1 and 2 is less because the object now moves through zone 1 first, which has the lesser time constant of decay, leading to a lesser maximum value for the input $I(t)$. *E*: model schematic: the input $I(t)$ is presented to our model neuron, which has both leak g_{leak} and voltage-gated calcium g_T conductances. The output directional bias DI_{out} is computed by comparing the peak voltage deflections caused by both inputs and is then compared with the input directional bias DI_{in} . *F*: output directional bias DI_{out} as a function of input directional bias DI_{in} for different values of the T-type calcium channel maximum conductance g_T . *G*: illustration of 3 different regimes. *1*) Both inputs cause voltage deflections that do not activate the T-type calcium conductance because their peak values are below its threshold (dashed line). *2*) The preferred input activates the T-type calcium conductance while the null input does not. *3*) Both inputs activate the T-type calcium conductance. *H*: the response of the model to the all 3 inputs described in *G*. In case 1 (*left*): both inputs do not trigger a calcium spike and the model output thus has a similar directional bias than the input. The model thus acts like a “follower”. In case 2 (*middle*): the preferred input causes a calcium spike, which greatly increases the output directional bias for a given nonzero input directional bias. The model thus acts like an “amplifier.” In case 3 (*right*): both inputs cause calcium spikes that are similar in shape, thereby causing a decrease in the output directional bias. The model thus acts like an “attenuator.” For the simulations, we used $A_n = 180$, $A_p = 310$, $g_T = 0.3 \mu S$.

The responses to these cases are shown in Fig. 2H. It is important to note that one can transition between these three regimes by varying multiple parameters in the model; here we are illustrating the case where I_{bias} is varied (Fig. 2H). In *case 1*, the responses are weakly or not at all affected by the conductance and the output directional bias will be similar to that of the input (Fig. 2H). The model behaves almost linearly and the output bias will be close to the input bias. In *case 2*, the input in the preferred direction activates the conductance, giving rise to a large voltage depolarization whereas the input in the null direction does not (Fig. 2H). The output bias is greater than the input bias and the model thus acts like an amplifier. In *case 3*, both inputs activate the conductance and both give rise to stereotyped voltage depolarizations. The output bias is less than the input bias (Fig. 2H) and the model therefore acts like an attenuator.

We next characterized the parameter regimes that gave rise to the three cases mentioned in the preceding text. Specifically, we looked at the effect of varying the input bias DI_{in} , the baseline current I_{bias} , and the maximum active conductance g_{T} . In all cases, we varied the input bias DI_{in} by increasing the amplitude of the larger input while keeping the amplitude of the smaller input constant.

Varying both DI_{in} and I_{bias} gave rise to different regimes (Fig. 3A): at very hyperpolarized voltages, a high-input directional bias DI_{in} is necessary to activate the active conductance and thereby make the model transition from the “linear” to the “amplifier” regime. The value of the directional bias DI_{in} at which this transition occurs decreases at more depolarized voltages. At more depolarized voltages, both inputs activate the active conductance and the model is in the “attenuator” regime.

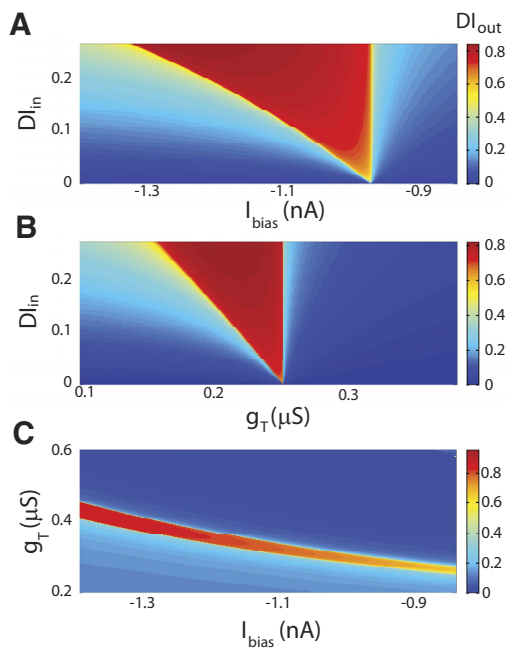


FIG. 3. Effects of varying the bias current I_{bias} , the T-type calcium channel conductance g_{T} , and the input directional bias DI_{in} on the output directional bias DI_{out} . DI_{in} was varied by increasing A_{p} while keeping $A_{\text{n}} = 280$. **A:** DI_{out} as a function of changing both DI_{in} and I_{bias} for $g_{\text{T}} = 0.3 \mu\text{S}$. **B:** DI_{out} as a function of changing both DI_{in} and g_{T} with $I_{\text{bias}} = -1.1 \text{ nA}$. **C:** DI_{out} as a function of changing both I_{bias} and g_{T} for $A_{\text{n}} = 280$ and $A_{\text{p}} = 310$, which corresponds to $DI_{\text{in}} = 0.0968$.

We note that even more depolarized voltages will lead to inactivation of the calcium conductance and that the model will then transition to the linear regime.

We next varied both the input directional bias DI_{in} by increasing the amplitude of the input in the preferred direction as well as the maximum active conductance g_{T} (Fig. 3B). For low values of g_{T} , a high-input directional bias DI_{in} is necessary to make the model transition from the linear to the amplifier regime. This value of input directional bias DI_{in} decreases for higher values of g_{T} . For high values of g_{T} , the model is in the attenuator regime as both inputs will activate the T-type conductance.

We also varied both the maximum active conductance g_{T} and the baseline current I_{bias} (Fig. 3C). We found that, for a given value of input directional bias DI_{in} , the value of g_{T} at which the transition from the linear to the amplifier regime decreases for increasing values of I_{bias} . These results show that different model parameters can change the values of input directional bias DI_{in} that is amplified by the T-type calcium conductance.

Nonlinear integration by subthreshold conductances is sufficient to account for the directional biases observed experimentally in TS neurons

We next explored whether nonlinear integration by subthreshold membrane conductances could account for the experimentally observed directional biases in TS neurons. We therefore combined our previously published model that incorporated different time constants of depression (described in the preceding text) with our current model that incorporates a nonlinear membrane conductance. As described previously, the depression time constants in the model were determined from experimental data as described previously (Chacron et al. 2009). The only model parameter that we systematically varied was the maximum conductance g_{T} . Furthermore, we used the same value of g_{T} . We used the same values of g_{T} for all neurons in our dataset.

Without an active conductance ($g_{\text{T}} = 0$), there was a strong and significant positive correlation between the predicted $|DSII|$ from our model and the experimentally measured value of $|DSII|$ ($R = 0.88$, $n = 18$, $P < 10^{-3}$; Fig. 4A). However, most datapoints were below the identity line (black line in Fig. 4A), indicating that our model with $g_{\text{T}} = 0$ systematically underestimated the directional bias. This could have been expected as all values of $|DSII|$ obtained from the model with $g_{\text{T}} = 0$ are < 0.5 (see preceding text for an explanation), whereas some neurons in our dataset had values of $|DSII|$ that were > 0.5 . We next partitioned our dataset into three groups: neurons for which $|DSII| < 0.15$, neurons for which $0.15 \leq |DSII| \leq 0.5$, and neurons for which $|DSII| > 0.5$ and compared the population-averaged predicted and experimentally measured values of $|DSII|$ for each group. Our results showed that the values of $|DSII|$ predicted by our model with $g_{\text{T}} = 0$ was significantly less than the experimentally measured value for groups 2 and 3 (Fig. 4B). This indicates that the discrepancy between model and data cannot fully be accounted by neurons for which $|DSII| > 0.5$. We will return to this point in the discussion.

We then activated the active conductance ($g_{\text{T}} = 0.3 \mu\text{S}$) and ran the model in the amplifier regime. This preserved the strong and significant positive correlation between the predicted $|DSII|$ values from our model and the experimentally measured value of $|DSII|$ ($R = 0.88$, $n = 18$, $P < 10^{-3}$; Fig. 4A). Also, the predicted values of $|DSII|$ were more quantita-

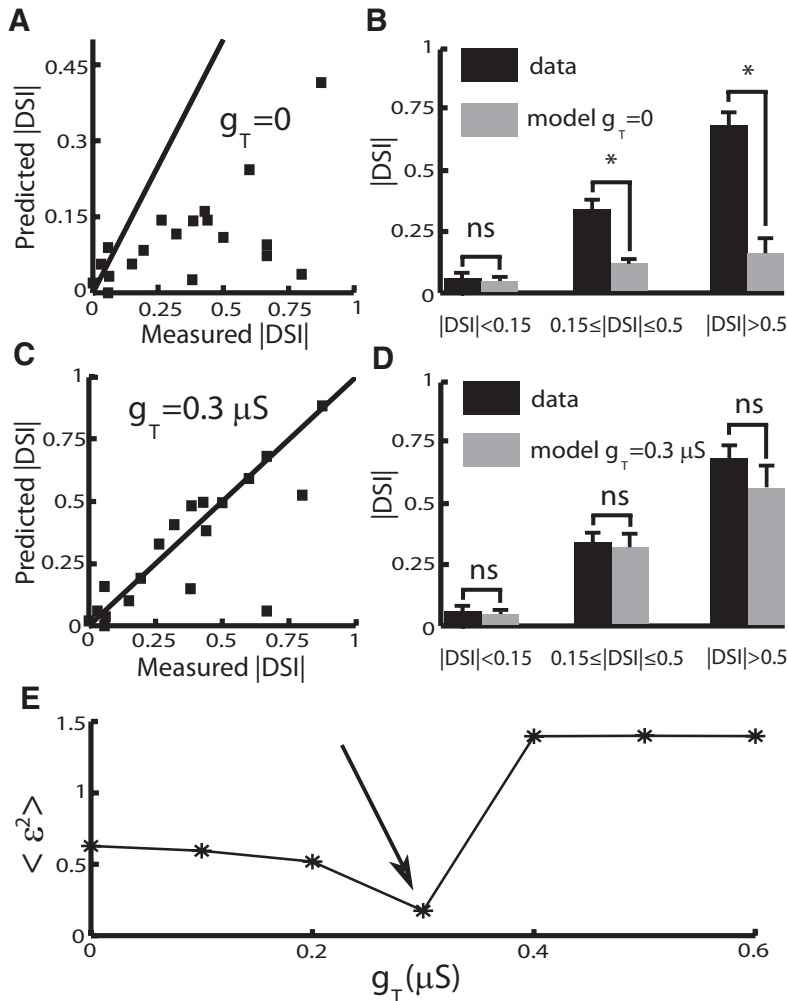


FIG. 4. A mathematical model incorporating both short-term synaptic depression and a nonlinear T-type conductance can account for experimentally measured values of directional selectivity. *A*: |DSII| predicted by our model (y axis) with no active conductance ($g_T = 0$) compared with the actual |DSII| measured experimentally (x axis). Although there is a significant positive correlation between both quantities ($R = 0.88$, $n = 18$, $P < 10^{-3}$), the predicted DSI underestimates the observed |DSII| in magnitude as most data points lie below the identity line (—). *B*: population-averaged DSI values predicted from the model with $g_T = 0$ (grey) and measured experimentally (black) for neurons whose experimentally measured |DSII| < 0.15 (left), $0.15 \leq |DSII| \leq 0.5$ (middle), and |DSII| > 0.5 (right). *C*: |DSII| predicted by our model with $g_T = 0.3 \mu\text{S}$ compared with the actual |DSII| measured experimentally. Both quantities are again strongly positively correlated ($R = 0.92$, $n = 18$, $P < 10^{-3}$). However, this model can quantitatively account for the observed directional selectivity in the population of TS neurons as most data points are close to the identity line (—). *D*: population-averaged DSI values predicted from the model with $g_T = 0.3 \mu\text{S}$ (grey) and measured experimentally (black) for neurons whose experimentally measured |DSII| < 0.15 (left), $0.15 \leq |DSII| \leq 0.5$ (middle), and |DSII| > 0.5 (right). *E*: mean square error (ϵ^2) between the model and data as a function of g_T . ns, the P value obtained using a sign-rank test was > 0.05 ; *, the P value obtained using a sign-rank test was < 0.01 . Throughout, we used $I_{\text{bias}} = -1.1 \text{ nA}$ for the model.

tively similar to those obtained experimentally (Fig. 4C). Our results showed that the values of |DSII| predicted by our model with $g_T = 0.3 \mu\text{S}$ were not significantly different from the experimentally measured ones for all three groups (Fig. 4D).

Finally, we quantified the goodness of fit between the model and data by computing the mean square error (ϵ^2) and plotted $\langle \epsilon^2 \rangle$ as a function of g_T . It is seen that $\langle \epsilon^2 \rangle$ is minimal when $g_T = 0.3 \mu\text{S}$ (Fig. 4E). This can be expected from the three regimes described in Fig. 2. When the model is in the linear regime ($g_T = 0$), there is a significant underestimation of the absolute directional bias |DSII| as described in the preceding text. Increasing g_T will cause the model to transition to the amplifier regime, which increases the |DSII| value from the model and gives a better fit to the data. However, further increasing g_T will cause the model to transition to the attenuator regime, which degrades the fit between data and model.

Subthreshold membrane conductances increase directional selectivity in TS neurons

Our models predict that nonlinear integration by subthreshold conductances not only act as the necessary nonlinear integrator but further can enhance the directional bias in TS neurons when activated preferentially by object motion in the neuron's preferred direction. We tested this hypothesis by

performing experiments in which we varied the resting membrane potential by varying the level of current injection through the recording electrode. Previous studies have shown that hyperpolarization by constant negative current injection can silence subthreshold membrane conductances in TS neurons (Fortune and Rose 1997, 2003), which should, based on our model, significantly reduce directional selectivity.

Figure 5A shows an example of a subthreshold depolarization with action potentials on top that can be de-activated by injecting hyperpolarizing current through the electrode. We first quantified the amplitude of these depolarizations as a function of the resting membrane potential value and found a maximum amplitude when the resting membrane potential was around -80 mV with more depolarized and more hyperpolarized giving rise to lower amplitudes (Fig. 5B).

We next looked at whether reducing the amplitude of these depolarizations had any effect on directional selectivity in TS neurons. Figure 5C shows the directional selectivity index DSI versus the holding current for an example neuron. This neuron was strongly directionally selective when no holding current was applied. However, hyperpolarization and depolarization both attenuated the value of |DSII| for this neuron as can be seen from the membrane potential response to a moving object (Fig. 5, D–F). Similar results were seen for other neurons. Overall,

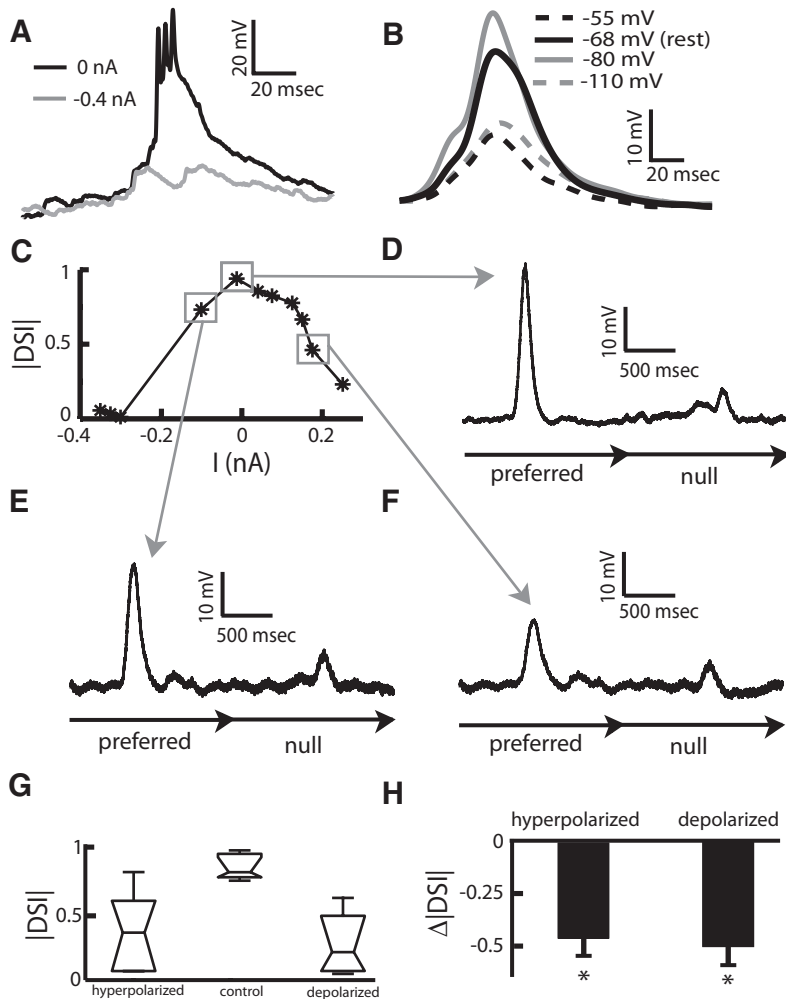


FIG. 5. Subthreshold membrane conductances influence directional selectivity in TS individual neurons. *A*: example subthreshold membrane depolarization caused by a subthreshold membrane conductance that can be silenced by intracellular current injection. *B*: the amplitude of these membrane depolarizations as a function of the resting membrane potential that was varied by current injection for an example TS neuron. Note that the traces were low-pass filtered to remove sodium action potentials. *C*: |DSII| vs. current injection for an example TS neuron. *D–F*: average low-pass filtered membrane potential traces in response to a moving object for this same neuron at 3 different levels of polarization. *G*: population averaged values of |DSII| under control, hyperpolarized, and depolarized conditions. |DSII| values under both hyper- and depolarized conditions were significantly different from under control conditions ($P = 0.0014$, 1-wave ANOVA, $n = 6$). *H*: Δ |DSII| was defined as the value of |DSII| under current injection minus the value of |DSII| for no current injection and was significantly different from 0 (hyperpolarization: $P = 0.00661$, Wilcoxon sign-rank test, $n = 6$; depolarization: $P = 0.00188$, Wilcoxon sign-rank test, $n = 6$).

|DSII| values obtained under hyper- and depolarized conditions were significantly less than those obtained under control conditions (Fig. 5*G*). The difference between the |DSII| values under hyper- and depolarized conditions and those obtained under control conditions were significantly different from zero (hyperpolarization: $P = 0.007$, Wilcoxon sign-rank test, $n = 6$; depolarization: $P = 0.002$, Wilcoxon sign-rank test, $n = 6$; Fig. 5*H*), thereby confirming that these subthreshold membrane conductances do influence directional selectivity in TS neurons.

How do these subthreshold conductances increase directional selectivity? Our model predicts that these conductances are preferentially activated when the object moves in the preferred direction. To test this hypothesis, we took advantage of the fact that subthreshold membrane conductances are “all-or-none” and can be de-activated in the neuron is hyperpolarized by negative DC current injection (Fortune and Rose 1997, 2003). We hyperpolarized TS neurons using negative DC current injection via the recording electrode.

The intracellularly recorded membrane potential response of a neuron to four consecutive cycles of the moving object is shown in Fig. 6*A* at a value of hyperpolarizing current near the threshold for de-activating the subthreshold conductance. In these trials, the amplitude of the response in the preferred direction (defined as the maximum value of the membrane potential minus its baseline activity) displays considerable

trial-to-trial variability (Fig. 6*A*, pluses): the subthreshold conductance was activated on two of the four trials. We plotted a histogram of the response amplitude values obtained when the object moved in the preferred direction for this neuron at this level of hyperpolarizing current and found a bimodal distribution with a clear separation threshold between the two modes (Fig. 6*B*). Note that nonzero variances of each mode in the histogram reflect the trial-to-trial variability displayed by TS neurons to a moving object. Stimulus trials for which the response amplitude was greater than the threshold were termed active trials as the subthreshold membrane conductance was activated. Stimulus trials for which the response amplitude was less than the threshold were termed passive trials.

The subthreshold membrane conductance was almost always activated by the moving object when no current was injected. Increasing the amount of hyperpolarizing current activated the subthreshold membrane conductance less and less frequently (Fig. 6*C*). We then set the value of hyperpolarizing current such that the conductance was activated on only half of the stimulus trials and then compared the trial-averaged membrane potential responses in the preferred and null directions for active and passive trials. Our results showed that, although the maximum response amplitude in the null direction was similar for both active and passive trials, nevertheless the maximum response ampli-

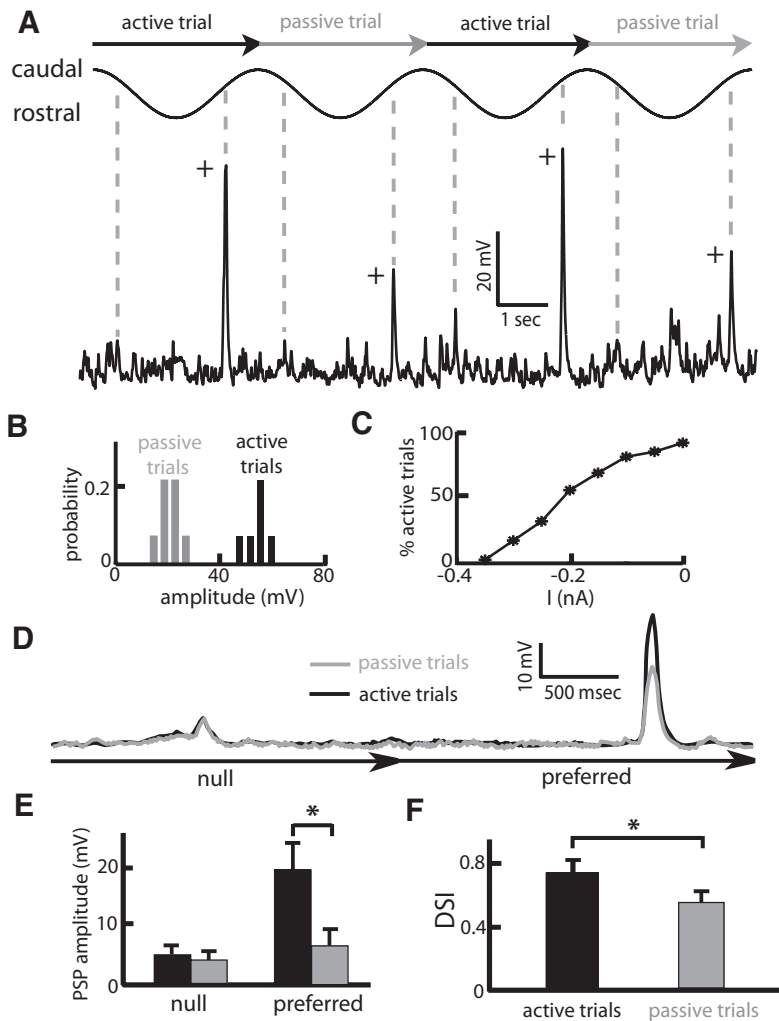


FIG. 6. Subthreshold membrane conductances are preferentially elicited when the object moves in the preferred direction. *A*: 4 consecutive cycles of object motion (*top*) and corresponding recorded low-pass filtered (finite impulse response filter in spike2, 200 Hz cutoff frequency) membrane potential (*bottom*) from an example neuron. Current injection of -0.2 nA was used to maintain the membrane potential of this neuron at a value such that there is considerable trial-to-trial variability in the peak response in the preferred direction as marked by the plus signs. *B*: a histogram of the response amplitude for this same neuron in the preferred direction shows a bimodal distribution with a clear separation threshold (black vertical line). Trials that gave rise to a response amplitude in the preferred direction that was greater than the threshold were termed “active” and those that did not were termed “passive.” *C*: percentage of active trials as a function of the holding current for this same neuron. *D*: the low-pass filtered membrane potential waveforms are shown averaged over active (black) and passive (gray) trials for $I = -0.2$ nA. It is seen that the depolarization is greater in the preferred direction for active trials. However, both traces are similar in the null direction. *E*: population-averaged response amplitudes of depolarizations for active (black) and passive (grey) trials were not significantly different in the null direction (pairwise *t*-test, $n = 7$, $P = 0.443$) but were significantly higher for active trials in the preferred direction (pairwise *t*-test, $n = 7$, $P = 0.004$). The response amplitude was computed as the maximum value of the membrane potential minus its baseline value. *F*: the absolute directional bias |DSI| was significantly greater for active trials (black) as compared with passive trials (grey; $P = 0.007$, Wilcoxon rank sum test, $n = 7$).

tude in the preferred direction was greater for active trials than for passive trials (Fig. 6D).

We repeated this procedure for six other neurons and again found a clear separation between response amplitudes when the subthreshold conductance was activated and those obtained when it was not. The response amplitudes of active and passive trials were not significantly different in the null direction ($P = 0.443$, pairwise *t*-test, $n = 7$), and the response amplitudes of active trials were significantly greater than that of passive trials in the preferred direction ($P = 0.004$, pairwise *t*-test, $n = 7$; Fig. 6E). The difference between the response amplitudes in the preferred direction led to a significantly greater |DSI| values computed from active trials only as compared with those computed from passive trials only ($P = 0.007$, Wilcoxon rank-sum test, $n = 7$; Fig. 6F). These results show that subthreshold membrane conductances in TS neurons are indeed preferentially activated when the object moves in the preferred direction, as predicted by our model, and increase |DSI|.

Subthreshold voltage-gated calcium channels increase directional selectivity in TS neurons

We next turned our attention toward elucidating the nature of these subthreshold membrane conductances. The depen-

dence of the active conductance on the level of polarization suggests that it is only active at low voltages within the range observed for T-type calcium channels (Fig. 5B) (Coulter et al. 1989). As such, we injected the T-type calcium channel antagonists NiCl_2 and Mib close to the recording site. Injection of NiCl_2 reduced the response amplitude in the preferred direction but not in the null direction (Fig. 7A), and similar results were seen with the more selective antagonist Mib. Both NiCl_2 and Mib significantly decreased the response amplitude in the preferred direction (pairwise *t*-test, $n = 5$, $P = 0.01$; Fig. 7B). Furthermore, both of these agents reduced directional selectivity in TS neurons, whereas control injections of saline alone, in contrast, had no significant effect on directional selectivity (Fig. 7C).

Effects of other channels on directional selectivity

Previous studies have shown that many TS neurons have sodium dependent subthreshold conductances that can enhance tuning properties (Fortune and Rose 2003). Therefore we tested whether these sodium conductances might enhance directional selectivity in a manner similar to that of T-type calcium channels by using the intracellular sodium channel antagonist QX-314. Our results showed that QX-314 eliminated spiking in TS neurons (Fig. 8A); this is consistent with previous

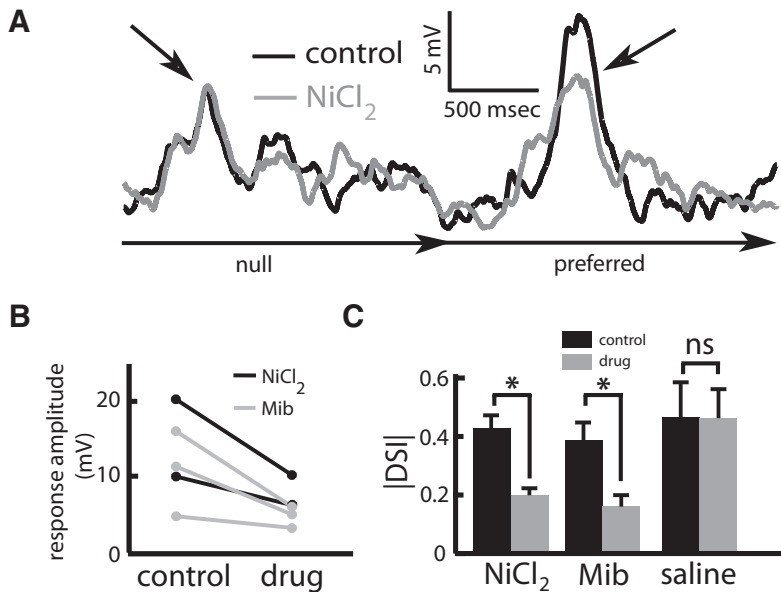


FIG. 7. Calcium-dependent channels enhance directional selectivity in TS neurons. *A*: averaged low-pass filtered (FIR filter in spike2, 30 Hz cutoff frequency) membrane potential response from an example neuron under control (black) and after injection of nickel chloride (NiCl₂). A decreased peak voltage depolarization is observed in the preferred direction (right arrow) while no change is seen in the null direction (left arrow). *B*: both NiCl₂ and mibefradil (Mib) reduced the amplitude of subthreshold depolarizations in TS neurons in the preferred direction. *C*: injection of both NiCl₂ and Mib significantly reduced directional selectivity in TS neurons whereas saline injection had no effect. Asterisk, statistical significance using a Wilcoxon ranksum test at the $P = 0.01$ level; ns, no statistical significance. For NiCl₂, we had $P \ll 10^{-3}$ and $df = 24$, whereas for Mib, we had $P = 0.0024$ and $df = 26$. For saline, we had $P = 0.9697$ and $df = 19$.

results (Fortune and Rose 2003). However, QX-314 did not affect the subthreshold membrane potential response of TS neurons to a moving object (Fig. 8*B*), and the |DSII| computed from the membrane potential response was not altered (*C*).

We also examined the role of chloride channels using the antagonist picrotoxin (PTX). PTX altered the baseline firing activity of TS neurons: the number of action potentials per unit time increased and these action potentials tended to form clusters ("bursts;" Fig. 9*A*). However, PTX did not affect the subthreshold membrane potential response of TS neurons to a moving object (Fig. 9*B*). Although the increased firing activity due to PTX could have altered directional selectivity, our results showed that this is not the case as the |DSII| values computed from the spike train under control conditions and those computed after PTX injection were not significantly different from one another (Fig. 9*C*).

Finally, we examined the role of NMDA receptors using the antagonist APV. APV caused a reduction in the baseline firing activity of TS neurons (Fig. 10*A*) but did not alter the subthreshold membrane potential response to a moving object (*B*). Although the reduced firing activity due to APV could have altered directional selectivity, the |DSII| values computed from the spike train under control conditions and those computed after APV injection were not significantly different from one another (Fig. 10*C*).

We note that the resting membrane potential values were not significantly affected by QX-314, PTX, and APV. Our results therefore show that the subthreshold voltage-gated conductances that lead to increased directional biases in TS neurons are blocked by calcium channel antagonists. As these conductances are active in the subthreshold regime, they are most likely mediated by T-type calcium channels. Our pharmacological results show that other conductances such as *N*-methyl-D-aspartate receptors (NMDARs), persistent sodium, or chloride channels do not mediate directional selectivity in TS neurons.

DISCUSSION

We have demonstrated a novel function of subthreshold membrane conductances in that they act as a nonlinear inte-

grator of spatiotemporal information for the generation of directionally selective responses. Our mathematical model has shown that these conductances can conserve, amplify, or attenuate a given directional bias depending on the level of polarization and relative amplitudes of PSPs. A variety of parameters, including the baseline current and maximum conductance value, can alter the range of input directional biases that can be conserved, amplified, or attenuated.

We then tested our model's prediction that the level of membrane polarization would alter directional selectivity using current injection through the recording electrode. We found that both de- and hyperpolarization can decrease directional selectivity in TS neurons in accordance with our model's predictions. Further, we compared active and passive stimulus trials to show that such conductances increased directional selectivity by increasing the response in the preferred direction only.

Finally, we applied a variety of pharmacological agents to identify the subthreshold conductance. The application of nickel or Mib reduced the amplitude of the membrane depolarizations caused by subthreshold membrane conductances and furthermore reduced directional selectivity in TS neurons, whereas other agents that target other conductances, including sodium, chloride, and NMDA, did not. Nickel and Mib are antagonists of T-type calcium channels, suggesting that these conductances are responsible for nonlinear integration in TS neurons was most likely a T-type calcium channel.

Subthreshold membrane conductances increase directional selectivity in sensory neurons

We have shown that subthreshold voltage-gated calcium channels act as a nonlinear integrator used in the generation of directionally biased responses in sensory neurons. As these conductances are ubiquitous in the CNS of vertebrates including mammalian visual cortex (Giffin et al. 1991; Salami and Fathollahi 2000), the novel function that we have demonstrated here could occur in other systems. Further, the mechanism by which this conductance acts as a nonlinear integrator for direction selectivity is different

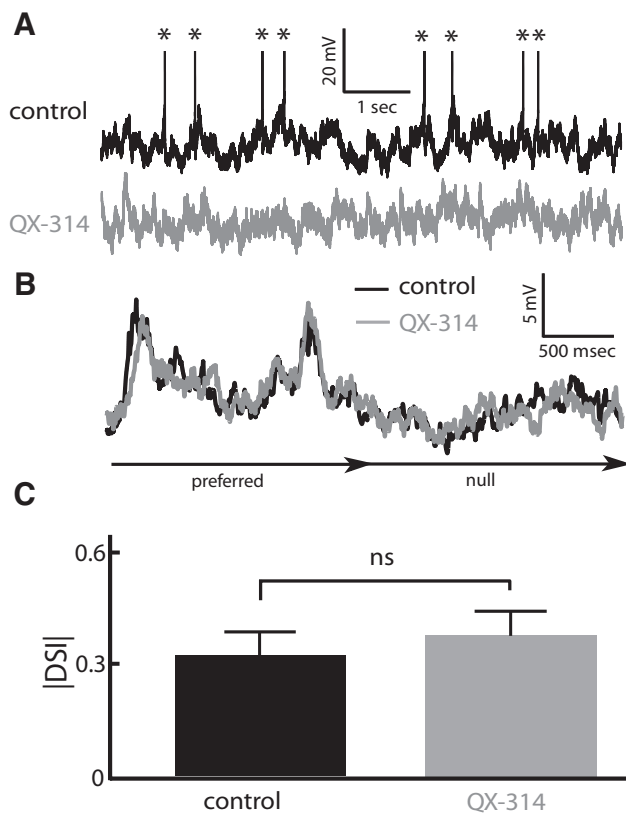


FIG. 8. The sodium channel antagonist QX-314 does not affect directional selectivity in TS neurons. *A*: example membrane potential recording from a neuron's baseline activity under control conditions (black) showing action potentials marked by asterisk. Note that the ~50 mV action potentials are truncated. The baseline activity from this same neuron did not show action potential firing in after application of QX-314 (gray). *B*: low-pass filtered (FIR filter in spike2, 30 Hz cutoff) membrane potential trace averaged over stimulus trials of this same neuron in response to a moving object under control (black) and after QX-314 (gray). Note that both traces almost completely overlap. *C*: population-averaged |DSII| values computed from the membrane potential under control and after QX-314 were not statistically significantly different from one another ($P = 0.7334$, sign-rank test, $n = 12$) as indicated (ns).

from previously proposed nonlinear integrators: subthreshold conductances actually enhance the response in the preferred direction via supralinear summation of synaptic input while other nonlinear integrators such as the spiking threshold work by suppressing the response in the null direction (Priebe and Ferster 2008; Priebe et al. 2004). The activation of these subthreshold conductances can lead to multiple action potentials rather than a single one as is the case for voltage-gated sodium channels. Although our data show that the spiking threshold does not enhance directional selectivity in TS neurons, the nonlinear integration by subthreshold membrane conductances and subsequent nonlinear integration by other mechanisms such as the spiking threshold and inhibition are not necessarily mutually exclusive and could also contribute to directional selectivity. Although our results indicate that other conductances do not seem to contribute to directional selectivity, we did not systematically vary the bias current injection to investigate the putative role of these conductances at other membrane potential levels. Such studies are beyond the scope of this paper.

Universality of nonlinear integration of synaptic input by subthreshold membrane conductances

The mechanism by which subthreshold membrane conductances nonlinearly integrate synaptic input is generic and acts via supralinear summation. The mechanism is similar to supralinear summation of synaptic input by other subthreshold conductances such as persistent sodium channels (Berman et al. 2001; Heckman et al. 2003; Schwandt and Crill 1995) or NMDA receptors (Rhodes 2006). Such nonlinear integration has been shown to serve a variety of functions including contrast enhancement (Dhingra et al. 2005) and high-frequency sensitivity to moving sensory images (Haag and Borst 1996). This similarity has important consequences. First, although our results have shown that persistent sodium channels and NMDA receptors did not contribute to enhancing directional selectivity in TS neurons, it is nevertheless possible that these channels could enhance directional selectivity in other systems via a mechanism similar to the one shown here. Second, it is possible that subthreshold voltage-gated calcium conductances could me-

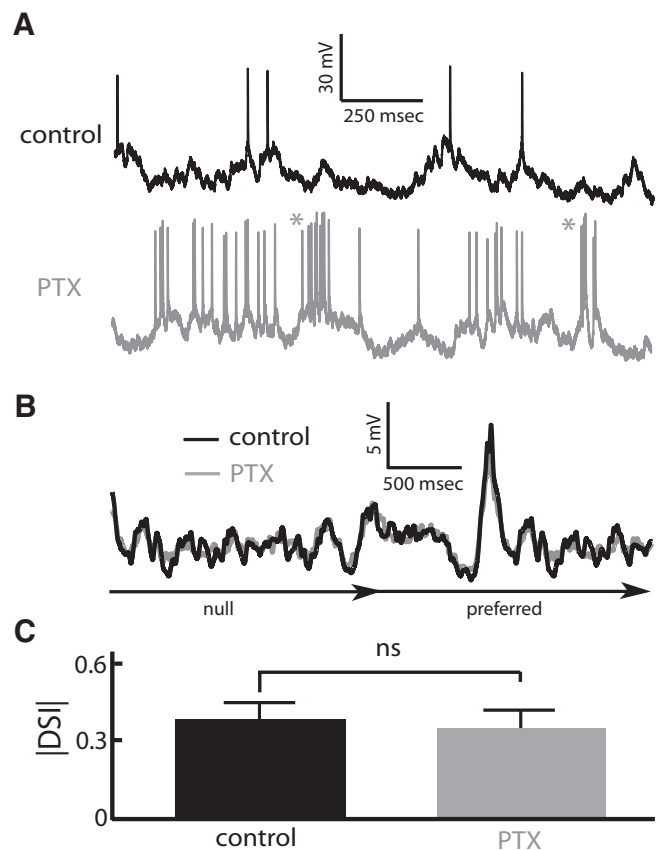


FIG. 9. The chloride channel antagonist picrotoxin (PTX) does not affect directional selectivity in TS neurons. *A*: example membrane potential recording from a neuron's baseline activity under control conditions (black). This same neuron showed elevated firing in its baseline activity as well as a greater propensity to fire bursts of action potentials (see asterisk) action potential firing after PTX (gray). *B*: low-pass filtered (FIR filter in spike2, 30 Hz cutoff) membrane potential trace of this same neuron in response averaged over stimulus trials to a moving object under control (black) and after PTX (gray). Note that both traces almost completely overlap. *C*: population-averaged |DSII| values computed from the membrane potential under control and after PTX injection were not statistically significantly different from one another ($P = 0.5469$, Wilcoxon rank-sum test, $df = 15$) as indicated (ns).

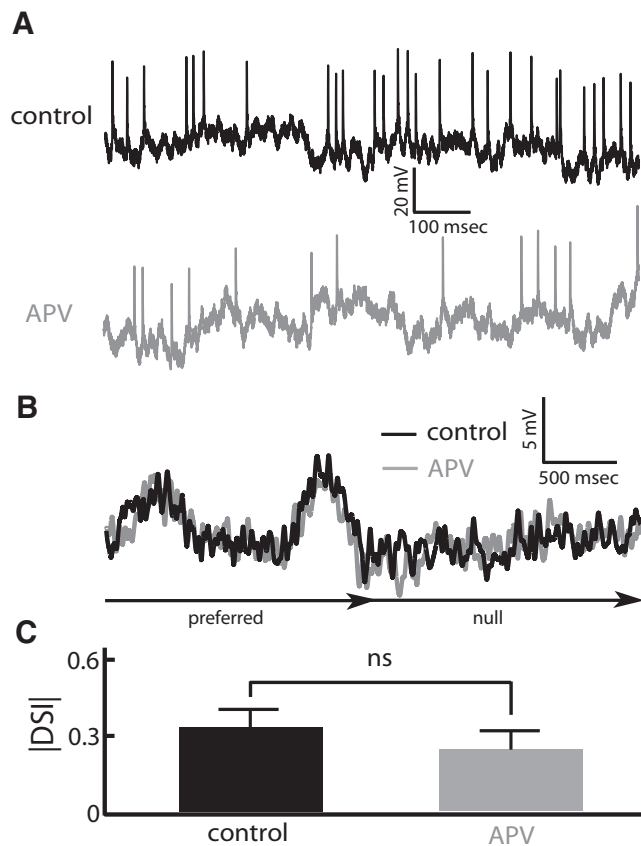


FIG. 10. The *N*-methyl-D-aspartate receptor antagonist 2-amino-5-phosphonovaleric acid (APV) does not affect directional selectivity in TS neurons. *A*: example membrane potential recording from a neuron's baseline activity under control conditions (black). This same neuron showed reduced baseline firing activity after APV (gray). *B*: low-pass filtered (FIR filter in spike2, 30 Hz cutoff) membrane potential trace of this same neuron averaged over stimulus trials in response to a moving object under control (black) and after APV (gray). Note that both traces almost completely overlap. *C*: population-averaged |DSII| values computed from the membrane potential under control and after APV injection were not statistically significantly different from one another ($P = 0.4105$, Wilcoxon rank-sum test, $df = 18$) as indicated (ns).

diate other computations via supralinear summation of synaptic input. For example, selectivity to ascending or descending frequency modulated acoustic sweeps has been observed in mammalian inferior colliculus (IC) and auditory cortex (Fuzessery and Hall 1996; Fuzessery et al. 2006; Razak and Fuzessery 2006, 2008; Suga 1965). As the IC is homologous to the TS, a comparison of the mechanisms that lead to directional selectivity in both structures is expected to be quite insightful.

Our mathematical model predicts that subthreshold conductances can sometimes attenuate a given bias in the input. Specifically, this occurs when inputs caused by movement in both the preferred and the null directions both activate the subthreshold conductance (Fig. 2). Although our experimental data show that this does not appear to occur in TS neurons under normal conditions, such a mechanism could be potentially used to reduce variability in the responses of neural populations and further studies are necessary to confirm or invalidate this hypothesis. Further studies are necessary to examine this hypothesis.

Nature of the subthreshold membrane conductance

Our results have shown that injection of NiCl_2 and Mib reduced the amplitude of calcium-dependent voltage depolarizations that were elicited while the object moved in the preferred direction. While NiCl_2 is a broad-spectrum calcium channel antagonist, Mib is likely to be specific for T-type calcium channels at the concentration used here (Bloodgood and Sabatini 2007; Mehrke et al. 1994). Together with our characterization of the voltage dependence of these subthreshold conductances, these results strongly suggest that the subthreshold conductance is mediated by T-type calcium channels. However, there is growing evidence that presynaptic T-type calcium channel can influence presynaptic vesicle exocytosis (Bao et al. 1998). It is therefore possible that both NiCl_2 and Mib acted primarily presynaptically and altered the time constants of synaptic depression, which would alter directional selectivity (Carver et al. 2008; Chacron et al. 2009; Chance et al. 1998). This possibility is unlikely here as these drugs reduced the response amplitude in the preferred direction in a manner similar to that seen when the subthreshold membrane conductance was deactivated via hyperpolarizing current injection. Further studies are however necessary to fully rule out the possibility that these drugs interfered with presynaptic mechanisms.

Generation of directional selectivity in TS neurons

Any motion detector requires at least two components: asymmetric filtering of at least two spatially distinct inputs and nonlinear interaction between these inputs (Borst and Egelhaaf 1990). For example, in the insect visual system, the asymmetric filtering takes the form of temporally delaying one input while the nonlinear interaction takes the form of coincidence detection. In weakly electric fish midbrain neurons, we have previously shown asymmetric filtering of spatially distinct inputs via differential time constants of depression (Chacron et al. 2009). Here we have shown that the nonlinear interaction of these inputs was achieved by subthreshold membrane conductances that were most likely T-type calcium channels. The mechanism by which TS neurons integrate nondirectionally selective input from afferent neurons to generate directionally biased responses thus constitutes a Reichardt detector (Reichardt 1969, 1987). These mechanisms are different from those found in the insect visual system and described in the preceding text (Borst and Egelhaaf 1990).

The stimuli used in this study had an average velocity of 10 cm/s, which is the average velocity of the animal during prey capture experiments (Nelson and MacIver 1999). Previous studies have shown that weakly electric fish can track movement at much lower velocities (Cowan and Fortune 2007). Further studies are necessary to study how directional selectivity in TS varies as a function of the moving object's velocity. Further, it is likely that the mechanisms uncovered previously will give rise to velocity tuning (Carver et al. 2008). Moreover, nonlinear integration of input via subthreshold voltage-gated calcium channels is likely to also be dependent on the object's velocity but further studies are needed to study this putative dependence.

Maintenance and regulation of directional selectivity

Organisms presumably use directionally selective neurons for motion perception that are involved in a variety of behaviors. For weakly electric fish, these behaviors include prey capture (Nelson and MacIver 1999) and stimulus tracking (Cowan and Fortune 2007). Our results have shown for the first time that directional selectivity of neurons can be altered through regulation of intrinsic membrane conductances. This has important consequences for the organism as such conductances are regulated via multiple agents including neuromodulators. In particular, previous studies have shown the presence of serotonergic inputs in TS (Johnston et al. 1990). Thus T-type calcium channels could be downregulated by serotonin (Sun and Dale 1997). Directional selectivity in TS neurons could therefore be tuned by regulation of subthreshold voltage-gated calcium channels. This is an interesting possibility in which neuromodulators could be used to alter directional selectivity based on the behavioral context.

ACKNOWLEDGMENTS

We thank G. Pollack, K. Cullen, R. Krahe, S. Musallam, C. Pack, J. Martinez-Trujillo, S. Carver, and N. Cowan for useful discussions and critical readings of the manuscript. B. Dirlikov assisted with some of the data collection.

GRANTS

This research was supported by National Science Foundation Grant 0543985 to E. S. Fortune, Grass Foundation funding to E. S. Fortune and M. J. Chacron, and funding from the Canadian Institute of Health Research, CFI, and CRC to M. J. Chacron.

DISCLOSURES

No conflicts of interest, financial or otherwise, are declared by the author(s).

REFERENCES

- Adelson EH, Bergen JR. Spatiotemporal energy models for the perception of motion. *J Opt Soc Am A Opt Image Sci* 2: 284–299, 1985.
- Bao J, Li JJ, Perl E. Differences in Ca²⁺ channels governing generation of miniature and evoked excitatory synaptic currents in spinal laminae I and II. *J Neurosci* 18: 8740–8750, 1998.
- Bastian J. Electrolocation. II. The effects of moving objects and other electrical stimuli on the activities of two categories of posterior lateral line lobe cells in *Apteronotus albifrons*. *J Comp Physiol [A]* 144: 481–494, 1981.
- Bastian J, Chacron MJ, Maler L. Receptive field organization determines pyramidal cell stimulus-encoding capability and spatial stimulus selectivity. *J Neurosci* 22: 4577–4590, 2002.
- Berman N, Dunn RJ, Maler L. Function of NMDA receptors and persistent sodium channels in a feedback pathway of the electrosensory system. *J Neurophysiol* 86: 1612–1621, 2001.
- Bloodgood BL, Sabatini BL. Nonlinear regulation of unitary synaptic signals by CaV(2.3) voltage-sensitive calcium channels located in dendritic spines. *Neuron* 53: 249–260, 2007.
- Borst A, Egelhaaf M. Principles of visual motion detection. *Trends Neurosci* 12: 297–306, 1989.
- Borst A, Egelhaaf M. Direction selectivity of blowfly motion-sensitive neurons is computed in a two-stage process. *Proc Natl Acad Sci USA* 87: 9363–9367, 1990.
- Carver S, Roth E, Cowan NJ, Fortune ES. Synaptic plasticity can produce and enhance direction selectivity. *PLoS Comput Biol* 4: e32, 2008.
- Chacron MJ. Nonlinear information processing in a model sensory system. *J Neurophysiol* 95: 2933–2946, 2006.
- Chacron MJ, Bastian J. Population coding by electrosensory neurons. *J Neurophysiol* 99: 1825–1835, 2008.
- Chacron MJ, Doiron B, Maler L, Longtin A, Bastian J. Non-classical receptive field mediates switch in a sensory neuron's frequency tuning. *Nature* 423: 77–81, 2003.
- Chacron MJ, Toporikova N, Fortune ES. Differences in the time course of short-term depression across receptive fields are correlated with directional selectivity in electrosensory neurons. *J Neurophysiol* 102: 3270–3279, 2009.
- Chance FS, Nelson SB, Abbott LF. Synaptic depression and the temporal response characteristics of V1 cells. *J Neurosci* 18: 4785–4799, 1998.
- Coulter DA, Huguenard JR, Prince DA. Calcium currents in rat thalamo-cortical relay neurones: kinetic properties of the transient, low-threshold current. *J Physiol* 414: 587–604, 1989.
- Cowan NJ, Fortune ES. The critical role of locomotion mechanics in decoding sensory systems. *J Neurosci* 27: 1123–1128, 2007.
- Dhingra NK, Freed MA, Smith RG. Voltage-gated sodium channels improve contrast sensitivity of a retinal ganglion cell. *J Neurosci* 25: 8097–8103, 2005.
- Euler T, Detwiler PB, Denk W. Directionally selective calcium signals in dendrites of starburst amacrine cells. *Nature* 418: 845–852, 2002.
- Fortune ES. The decoding of electrosensory systems. *Curr Opin Neurobiol* 16: 474–480, 2006.
- Fortune ES, Rose GJ. Passive and active membrane properties contribute to the temporal filtering properties of midbrain neurons in vivo. *J Neurosci* 17: 3815–3825, 1997.
- Fortune ES, Rose GJ. Short-term synaptic plasticity contributes to the temporal filtering of electrosensory information. *J Neurosci* 20: 7122–7130, 2000.
- Fortune ES, Rose GJ. Voltage-gated Na⁺ channels enhance the temporal filtering properties of electrosensory neurons in the torus. *J Neurophysiol* 90: 924–929, 2003.
- Fuzessery ZM, Hall JC. Role of GABA in shaping frequency tuning and creating FM sweep selectivity in the inferior colliculus. *J Neurophysiol* 76: 1059–1073, 1996.
- Fuzessery ZM, Richardson MD, Coburn MS. Neural mechanisms underlying selectivity for the rate and direction of frequency-modulated sweeps in the inferior colliculus of the pallid bat. *J Neurophysiol* 96: 1320–1336, 2006.
- Giffin K, Solomon JS, Burkhalter A, Nerbonne JM. Differential expression of voltage-gated calcium channels in identified visual cortical neurons. *Neuron* 6: 321–332, 1991.
- Haag J, Borst A. Amplification of high-frequency synaptic inputs by active dendritic membrane processes. *Nature* 379: 639–641, 1996.
- Haag J, Denk W, Borst A. Fly motion vision is based on Reichardt detectors regardless of the signal-to-noise ratio. *Proc Natl Acad Sci USA* 101: 16333–16338, 2004.
- Heckman CJ, Lee RH, Brownstone RM. Hyperexcitable dendrites in motoneurons and their neuromodulatory control during motor behavior. *Trends Neurosci* 26: 688–695, 2003.
- Hitschfeld EM, Stamper SA, Vonderschen K, Fortune ES, Chacron MJ. Effects of restraint and immobilization on electrosensory behaviors of weakly electric fish *ILAR J* 50: 361–372, 2009.
- Hubel DH, Wiesel TN. Receptive fields, binocular interaction and functional architecture in the cat's visual cortex. *J Physiol* 160: 106–154, 1962.
- Inomata N, Tokutomi N, Oyama Y, Akaike N. Intracellular picrotoxin blocks pentobarbital-gated chloride conductance. *Neurosci Res* 6: 72–75, 1988.
- Jagadeesh B, Wheat HS, Kontsevich LL, Tyler CW, Ferster D. Direction selectivity of synaptic potentials in simple cells of the cat visual cortex. *J Neurophysiol* 78: 2772–2789, 1997.
- Johnston SA, Maler L, Tinner B. The distribution of serotonin in the brain of *Apteronotus leptorhynchus*: an immunohistochemical study. *J Chem Neuroanat* 3: 429–465, 1990.
- Maler L, Sas E, Johnston S, Ellis W. An atlas of the brain of the weakly electric fish *Apteronotus leptorhynchus*. *J Chem Neuroanat* 4: 1–38, 1991.
- Mehaffey WH, Ellis LD, Krahe R, Dunn RJ, Chacron MJ. Ionic and neuromodulatory regulation of burst discharge controls frequency tuning. *J Physiol* 102: 195–208, 2008.
- Mehrke G, Zong XG, Flockerzi V, Hofmann F. The Ca(++)-channel blocker Ro 40–5967 blocks differently T-type and L-type Ca++ channels. *J Pharmacol Exp Therap* 271: 1483–1488, 1994.
- Nelson ME, MacIver MA. Prey capture in the weakly electric fish *Apteronotus albifrons*: sensory acquisition strategies and electrosensory consequences. *J Exp Biol* 202: 1195–1203, 1999.
- Priebe NJ, Ferster D. Inhibition, spike threshold, and stimulus selectivity in primary visual cortex. *Neuron* 57: 482–497, 2008.

- Priebe NJ, Mechler F, Carandini M, Ferster D.** The contribution of spike threshold to the dichotomy of cortical simple and complex cells. *Nat Neurosci* 7: 1113–1122, 2004.
- Ramcharitar JU, Tan EW, Fortune ES.** Effects of global electrosensory signals on motion processing in the midbrain of *Eigenmannia*. *J Comp Physiol A Sens Neural Behav Physiol* 191: 865–872, 2005.
- Ramcharitar JU, Tan EW, Fortune ES.** Global electrosensory oscillations enhance directional responses of midbrain neurons in *Eigenmannia*. *J Neurophysiol* 96: 2319–2326, 2006.
- Razak KA, Fuzessery ZM.** Neural mechanisms underlying selectivity for the rate and direction of frequency-modulated sweeps in the auditory cortex of the pallid bat. *J Neurophysiol* 96: 1303–1319, 2006.
- Razak KA, Fuzessery ZM.** Facilitatory mechanisms underlying selectivity for the direction and rate of frequency modulated sweeps in the auditory cortex. *J Neurosci* 28: 9806–9816, 2008.
- Reichardt W, editor.** *Movement Perception in Insects*. New York: Academic, 1969.
- Reichardt W.** Evaluation of optical motion information by movement detectors. *J Comp Physiol [A]* 161: 533–547, 1987.
- Reichardt W, Wenking H.** Optical detection and fixation of objects by fixed flying flies. *Naturwissenschaften* 56: 424–425, 1969.
- Rhodes P.** The properties and implications of NMDA spikes in neocortical pyramidal cells. *J Neurosci* 26: 6704–6715, 2006.
- Rose GJ, Fortune ES.** New techniques for making whole-cell recordings from CNS neurons in vivo. *Neurosci Res* 26: 89–94, 1996.
- Rush ME, Rinzel J.** Analysis of bursting in a thalamic neuron model. *Biol Cybern* 71: 281–291, 1994.
- Salami M, Fathollahi Y.** Do Ca^{2+} channels share NMDA receptors in plasticity of synaptic transmission in the rat visual cortex? *Neuroreport* 11: 3887–3891, 2000.
- Schwindt PC, Crill WE.** Amplification of synaptic current by persistent sodium conductance in apical dendrite of neocortical neurons. *J Neurophysiol* 74: 2220–2224, 1995.
- Srinivasan MV, Poteser M, Kral K.** Motion detection in insect orientation and navigation. *Vision Res* 39: 2749–2766, 1999.
- Suga N.** Analysis of frequency-modulated sounds by auditory neurons of echo-locating bats. *J Physiol* 179: 26–53, 1965.
- Sun QQ, Dale N.** Serotonergic inhibition of the T-type and high voltage-activated Ca^{2+} currents in the primary sensory neurons of *Xenopus* larvae. *J Neurosci* 17: 6839–6849, 1997.
- Toporikova N, and Chacron MJ.** Dendritic SK channels gate information processing in vivo by regulating an intrinsic bursting mechanism seen in vitro. *J Neurophysiol* 102: 2273–2287, 2009.
- Turner RW, Maler L, Deerinck T, Levinson SR, Ellisman MH.** TTX-sensitive dendritic sodium channels underlie oscillatory discharge in a vertebrate sensory neuron. *J Neurosci* 14: 6453–6471, 1994.